

Robust shallow shadows

Renato M. S. Farias,^{1,2,*} Raghavendra D. Peddinti,¹ Ingo Roth,¹ and Leandro Aolita¹

¹*Quantum Research Center, Technology Innovation Institute, Abu Dhabi, UAE*

²*Instituto de Física, Universidade Federal do Rio de Janeiro, P.O. Box 68528, Rio de Janeiro, Rio de Janeiro 21941-972, Brazil*

We present a robust shadow estimation protocol for wide classes of shallow measurement circuits that mitigates noise as long as the effective measurement map is locally unitarily invariant. This is in practice an excellent approximation, encompassing for instance the case of ideal single-qubit Clifford gates composing the first circuit layer of an otherwise arbitrary circuit architecture and even non-Markovian, gate-dependent noise in the rest of the circuit. We argue that for approximately local noise the measurement channel has an efficient matrix-product (tensor-train) representation, and show how to estimate this directly from experimental data using tensor-network tools, eliminating the need for analytical or numeric calculations. We illustrate the relevance of our method with both numerics and proof-of-principle experiments on an IBM Q device. Numerically, we show that, while unmitigated shallow shadows with noisy circuits become more biased as the depth increases, robust ones become more accurate for relevant parameter regimes. Experimentally, we observe major bias reductions in two simple fidelity estimation tasks using 5-qubit circuits with up to 2 layers of entangling gates using the mitigated variant, of close to an order of magnitude for 10^4 measurement shots, e.g. Under the practical constraints of current and near-term noisy quantum devices, our method maximally realizes the potential of shadow estimation with global rotations.

Introduction. Randomized measurements are a central tool for the estimation of observables on repeatedly prepared quantum states [1–3]. Applications abound [4–15]. Ref. [16] derived guarantees and proved optimality of linear estimation from bases measurements generated by global or local Clifford rotations and coined the term “classical shadows”. Besides optimality, an important contribution of Ref. [16] is the efficiency of estimation from global Clifford rotations. For example, with the same classical shadow from constantly many state copies in the system size n , one can estimate many different pure state fidelities. In practice, however, harnessing this efficiency is typically not possible, since global Clifford rotations require the accurate implementation of “long” circuits of $\mathcal{O}(n^2/\log(n))$ many local gates [17]. This obstacle has motivated the study of “shallow shadows”, where shorter circuits are employed to “interpolate” between local and global rotations [18–22].

While the two-design property of uniformly random Clifford rotations allows for straight-forward analytical inversion of the effective measurement map [23], a prerequisite to construct the classical shadow, the works on shallow circuits resort to numerical evaluation of the effective measurement map for depth larger than two [21]. However, for measurement circuits involving entangling gates, noise and (calibration) errors will typically cause sizeable biases in the derived estimators on current noisy intermediate-scale quantum (NISQ) hardware. For this reason, using shallow circuits for precise estimations in practice unavoidably requires a variant of classical shadows that mitigates circuit noise. That such a mitigation is possible for classical shadows with single-qubit or global random Clifford rotations if the noise is well-characterized was shown for simple depolarizing noise models [24], local gate-dependent noise models [25], and

via randomized benchmarking experiments [26]. Going beyond these works, ideally one wishes a robust shadow scheme that replaces analytical or numerical calculations of the measurement map by a direct empirical estimation of it in the presence of noise. Such a tool was developed in Ref. [27], again for the cases of single-qubit or global random Clifford rotations under the assumptions of gate-independent Markovian after-gate noise. However, an extension to the most crucial, experimentally-relevant regime of shallow circuits, where no analytical calculation of the measurement frame is in general available, is missing.

We explore this territory. We present a robust shadow estimation scheme for shallow circuits with arbitrary architectures of random local gates, under mild noise-type assumptions. We assume only that the average measurement channel is invariant under single-qubit Clifford rotations and accurate implementation of a single initial state. A simple but experimentally-crucial observation is that, for this to happen, it is sufficient for instance that the first circuit layer consists of ideal single-qubit random Cliffords, regardless of the subsequent circuit, which can even be subject to (time-stationary) gate-dependent, non-Markovian noise. Single-qubit Clifford invariance guarantees that the measurement map is Pauli diagonal. In turn, the circuit shallowness guarantees that the corresponding diagonal elements admit a tensor train (TT) description of low-rank if the noise is only weakly correlated. This allows us to develop efficient methods for directly estimating the measurement channel using standard tensor-network tools such as the modified alternating least squares (MALS) [28].

We numerically quantify how unmitigated shadow estimations (of both fidelities and Pauli observables) in the presence of noise become increasingly biased as the

circuit depth increases. In contrast, we show that, for experimentally-relevant regimes, robust shallow shadows become more precise as the depth increases up to an optimal depth depending on the strength of the incoherence noise. For instance, for depth $D = 2$, we observe average fidelity estimation errors over random target states almost one order of magnitude larger for the unmitigated estimations than for the robust ones already at $n = 8$ qubits. Moreover, we apply our scheme to a recent experiment [5] where ideal, 4-qubit global Cliffords were approximated by depth-5 noisy circuits, in an unmitigated fidelity estimation. In numerical simulations, we observe a four-fold infidelity reduction with our method. Finally, we perform a proof-of-principle experiment on the `ibm_nairobi` device. We estimate the measurement frame on 5-qubit circuits of up to 2 layers of entangling gates, confirming significant deviations relative to the noiseless one. With this, we compare mitigated and unmitigated shadows in two simple fidelity estimation tasks. We observe major bias reductions using the robust variant, of close to an order of magnitude for 10^4 measurements, e.g. Our framework offers a versatile and practical solution to classical shadows in the most relevant regime for near-term quantum devices, where randomized measurements are implemented by noisy shallow circuits.

Note that a related line of research studies the problem of mitigating the noise in the state-preparation using non-linear shadow estimation [9, 29–31] or existing error-mitigation techniques [32].

Robust classical shadows. We start by reviewing the classical shadow protocol on an ideal noiseless device. Consider a quantum device that can be repeatedly prepared in an unknown n -qubit quantum state ϱ . Furthermore, we will work with a quantum device that is capable of implementing circuits composed from a unitary gate set \mathcal{G} and of performing a measurement in a fixed (computational) basis, specified by the effects $\mathcal{B} = \{\Pi_z = |z\rangle\langle z|\}_{z \in [d]}$, with $d = 2^n$ and $[d] = \{0, 1, \dots, d-1\}$.

A probability measure ν on the unitary group $U(d)$ with support in the implementable circuits defines an ensemble of random bases measurements. The corresponding *measurement protocol on an input state ϱ* repeats the following primitive: (i) draw $g \sim \nu$; (ii) prepare ϱ , apply g , and perform the measurement \mathcal{B} ; (iii) observing measurement outcome z , record the tuple (z, g) . The output of the data acquisition is a sequence $\mathcal{S} = \{(z_k, g_k)\}_{k=1, \dots, |\mathcal{S}|}$, with $|\mathcal{S}|$ the cardinality of \mathcal{S} .

Every iteration of the protocol is described by the same positive operator-valued measure (POVM) taking values $\Pi_{z,g} = g^\dagger \Pi_z g$ with g in the support of ν and $z \in [d]$. If the support of ν is sufficiently large, the POVM is informationally-complete (IC) and asymptotically any information about ϱ can be reconstructed from the measurement statistic \mathcal{S} .

To be instructive, in the following we restrict ourselves to the simplest task of estimating a linear functional

$(O|\varrho) = \text{Tr}[O^\dagger \varrho]$, here defined as the Hilbert-Schmidt inner product with an endomorphism O of \mathbb{C}^d . Examples include the estimation of the fidelity of ϱ with respect to a pure target state $O = |\psi\rangle\langle\psi|$ or multi-qubit Pauli observables. The robust shallow shadows explored in our work can also be readily employed in non-linear estimation (see e.g. Ref. [33]).

Given \mathcal{S} , an estimator for $(O|\varrho)$ can be constructed via standard linear inversion [34]: Consider the frame operator of the measurement POVM, also known as the effective measurement map,

$$S = \mathbb{E}_{g \sim \nu} \left[\sum_{z \in [d]} |\Pi_{z,g}\rangle\langle\Pi_{z,g}| \right], \quad (1)$$

where we have used Dirac notation with respect to the Hilbert-Schmidt inner product. Since the POVM is informationally complete (IC), S is invertible and the elements of the canonical dual frame are given by $\bar{\Pi}_{z,g} = S^{-1}(\Pi_{z,g})$, fulfilling $\mathbb{E}_{g \sim \nu} \left[\sum_{z \in [d]} |\bar{\Pi}_{z,g}\rangle\langle\bar{\Pi}_{z,g}| \right] = S^{-1}S = \mathbb{1}_{d^2}$, with $\mathbb{1}_{d^2}$ being the $d^2 \times d^2$ identity operator. In the classical post-processing, we evaluate the scalar function $o(z, g) = (O|\bar{\Pi}_{z,g})$ on each entry of \mathcal{S} and take the empirical mean $\hat{o} = \sum_{(z,g) \in \mathcal{S}} o(z, g)$. For the ideal device, we observe (z, g) with probability density $p(z, g) = (\Pi_{z,g}|\varrho) d\nu(g)$ and, thus, \hat{o} is indeed an unbiased estimator of

$$\mathbb{E}_{z,g}(\hat{o}) = \mathbb{E}_{g \sim \nu} \left[\sum_{z \in [d]} (O|\bar{\Pi}_{z,g})\langle\Pi_{z,g}|\varrho| \right] = (O|\varrho). \quad (2)$$

In practice, however, experimental imperfections in the implementation of the basis measurement \mathcal{B} and the circuits in the support of ν induce a bias in the estimator. We denote by $\tilde{\Pi}_{z,g}$ the elements of the POVM that is actually implemented on the device and define the “one-sided” *noisy frame operator* as

$$\tilde{S} = \mathbb{E}_{g \sim \nu} \left[\sum_{z \in [d]} |\Pi_{z,g}\rangle\langle\tilde{\Pi}_{z,g}| \right]. \quad (3)$$

The same argument above now yields a non-vanishing estimator bias such that $\text{bias}(O, \varrho) = |\mathbb{E}(\hat{o}) - (O|\varrho)| = |(O|S^{-1}\tilde{S} - \text{Id}_{d^2}|\varrho)|$.

The form of the bias already hints at a conceptionally simple solution to mitigate the noise. Assume we have an empirical estimate of the noisy frame operator \tilde{S} and it is still invertible, which happens if $\{\tilde{\Pi}_{z,g}\}_{z,g}$ is still informationally complete. We can make use of this estimate in the construction of a scalar function $\tilde{o}(z, g) = (O|\tilde{S}^{-1}|\Pi_{z,g})$ that we evaluate instead of $o(z, g)$ in the classical post-processing. The resulting mean estimator \hat{o} is again unbiased with $\mathbb{E}(\hat{o}) = (O|\tilde{S}^{-1}\tilde{S}|\varrho)$.

When ν is the uniform measure over the multi-qubit Clifford group, the ideal frame operator S takes the particular simple form of a global depolarizing channel with

effective depolarization strength $1/(d + 1)$ [23]. The simple structure becomes apparent when realizing that S is a channel twirl of the dephasing channel $\mathcal{M} = \sum_{z \in [d]} |\Pi_z\rangle\langle \Pi_z|$ that describes the computational basis measurement. For the Clifford group, a unitary 2-design, S commutes with arbitrary unitary channels [35]. If ν is the uniform measure on the n -fold tensor product of single-qubit Clifford unitaries, S is only invariant under local one-qubit unitary gates. Since \mathcal{M} is the tensor-product of local dephasing channels, the projection of \mathcal{M} onto the locally unitarily invariant subspace is the product of local depolarizing channels.

If the noise does not break the measures' invariance property, \tilde{S} has the same structure as S , a global (linear span of local) depolarizing channel(s) for ν the uniform measure over the global (local) Clifford group. This insight is at the heart of the robust shadows introduced in Ref. [27]. There, the invariance assumption is justified by assuming a noise channel Λ acting *directly before the measurement* and *independent* of the unitary rotation g that is implemented. Under this assumption, \tilde{S} simply is the ideal channel twirl of the concatenation of the dephasing channel and the noise channel.

More concretely, recall that conjugation with the Clifford group (as with the unitary group) acts irreducibly on the space of traceless matrices, e.g. [2]. Correspondingly, tensor-products of single-qubit Clifford channels decompose into d irreducible representations (*irreps*) without multiplicities labelled by $k \in \{0, 1\}^n$. The projectors onto the irreps are $\Phi_k = \bigotimes_{l \in [n]} \Phi_{k_l}$ with $\Phi_0 = d^{-2} |\mathbb{1}_2\rangle\langle \mathbb{1}_2|$ and $\Phi_1 = \mathbb{1}_4 - \Phi_0$. Assuming single-qubit Clifford-invariance, the noisy frame operator can, thus, be written as

$$\tilde{S} = \sum_{k \in \{0, 1\}^n} f_k \Phi_k \quad (4)$$

with coefficients $f_k \in \mathbb{R}$.

Ref. [27] proposed the following *calibration procedure* to learn the coefficients f_k : Perform a randomized bases measurement on the input state $|0\rangle\langle 0|$. The post-processing is analogous to that for linear shadow estimation. But here we evaluate the scalar function

$$\phi_k(z, g) = (Z_k | \Pi_{z,g}) \quad (5)$$

with $Z_k = \bigotimes_{l \in [n]} Z^{k_l}$ and Z the Pauli-Z operator. In contrast to the scalar function o , ϕ does not use the dual frame. Assuming the initial state $|0\rangle\langle 0|$ can be accurately prepared, the mean of ϕ_k evaluated on \mathcal{S} is an unbiased estimator for f_k .

Results. The starting observation for our work is the following: Let ν be an arbitrary random ensemble of quantum circuits whose implementation suffers time-stationary, gate-dependent noise and errors. The noise can be non-Markovian. If the first gate layer of the circuits, that is applied to the state under scrutiny, accurately implements local channel twirls, then \tilde{S} in Eq. (3)

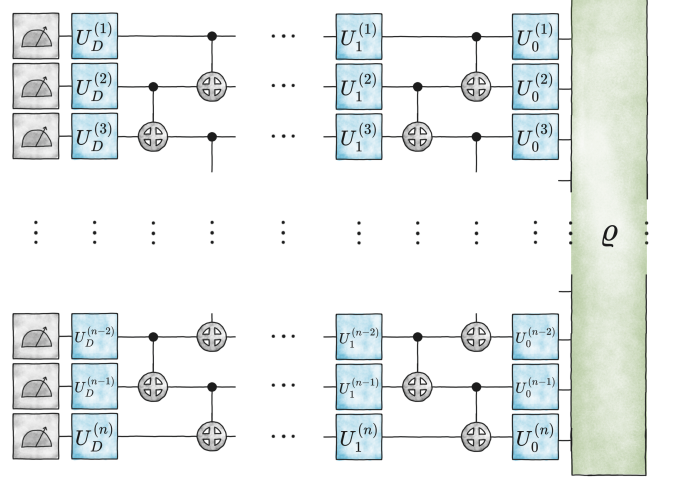


FIG. 1. **Hardware-efficient circuits for robust shallow shadows.** Given an initial state ϱ , the circuit implementing the measurement consists of $(D + 1)$ random layers. For $D = 0$, only a layer of n single-qubit rotations is present. Each extra layer is composed of a sub-layer of entangling gates followed by n single-qubit rotations. At the end, a computational basis measurement is performed.

still has the structure of Eq. (4). Hence, \tilde{S} can be estimated via the above calibration procedure introduced for local Clifford rotations in Ref. [27]. A practically motivated assumption is that the major source of noise in the implemented circuits are entangling gates and readout noise. If the first layer then consist of accurately implemented Haar random unitary or Clifford single qubit gates, the invariance assumption holds.

Circuits and tensor network methods. If the quantum circuit implementing g has low depth, we can make use of tensor network methods at multiple places of the protocol in order to reduce the runtime and storage complexity of the calibration protocol as well as partially for the estimation protocol. To be concrete, we specify a circuit ensemble that is directly motivated by existing hardware architectures and applications. The circuit architecture we use is based on the so-called *hardware-efficient ansatz* [36], depicted in Fig. 1. The circuit starts with a layer of single-qubit rotations, i.i.d. sampled from the Haar measure on single-qubit unitaries or Clifford unitaries. This layer is labelled as depth $D = 0$. Every subsequent layer is composed of a “sub-layer” of entangling gates followed by another sub-layer of single-qubit rotations sampled from the same measure as before. In principle, for the subsequent single qubit layers also other measures are admissible.

The entangling layer of the hardware-efficient ansatz has a matrix-product operator (MPO) representation of bond dimension $\chi_C = 2$, see App. C. Thus, $\Pi_{z,g}$ for g of depth D is exactly described by a matrix-product state (MPS) — also known as tensor train (TT) — of

bond dimension (TT-rank) χ_C^D . As a consequence, also the vector of scalar functions $\phi(z, g) = (\phi_k(z, g))_{k \in [n]}$ is described by a TT of rank at most χ_C^{2D} and can be efficiently computed and stored for every observed tuple (z, g) .

Furthermore, if the noise does not introduce sizeable non-local correlation, also \tilde{S} has an efficient tensor representation and the coefficient vector $f = (f_k)_{k \in [n]} \in \mathbb{R}^n$ is given by a low-rank TT. We illustrate this argument with a specific noise model in App. C. In particular, for single-qubit Pauli noise, the TT-rank of f is at most $\chi = 4^D$. This justifies to formulate the post-processing of the calibration procedure as the TT recovery problem

$$f = \arg \min_{f' \text{ rank-}\chi \text{ TT}} \left\| \frac{1}{|\mathcal{S}|} \sum_{(z, g) \in \mathcal{S}} \phi(z, g) - f' \right\|_{\ell_2}, \quad (6)$$

i.e. the problem of fitting an average of low-rank TTs with a TT of low-rank.

Standard approaches for tensor recovery such as modified alternating least-square optimization (MALS) [28] can be readily adopted. In particular, for MALS, we can perform the local update step for every core using contractions and pseudo-inverses with storage and time complexity scaling polynomial in the system size, TT ranks, and number of samples. This suggests that for sufficiently local noise and shallow circuits \tilde{S} can be efficiently learned. Below, we take this as a motivation to numerically investigate the performance of the scheme using MALS. Note, however, that showing overall efficiency would additionally require to prove a guarantee for the TT recovery algorithms from \mathcal{S} with polynomial cardinality.

The construction of the dual frame for the estimation protocol requires the inverse of \tilde{S} . Since Eq. (4) is an orthogonal decomposition, $\tilde{S}^{-1} = \sum_{k \in \{0,1\}^n} (f_k)^{-1} \Phi_k$. Even though f is a low-rank TT, its element-wise inverse f^{-1} might have higher rank. Nonetheless, one can attempt to find a low-rank TT description either from an estimate for f or directly from the data using the TT recovery algorithms.

Numerical results. Here, we numerically study the performance of robust estimation with shallow circuits using architectures that are motivated by applications. We use two noise models: (i) two-qubit *incoherent* noise model, where a different unitary noise is applied to a circuit at each execution (see App. A for details); (ii) a composition of a two-qubit Pauli noise with *gate-dependent* single-qubit Pauli noise, where different single-qubit gates suffer from different Pauli noise channels.

We begin by assessing the need of mitigating noise in shallow circuits. The top panel of Fig. 2 shows the worst-case bias, $\max_{O, \varrho} \text{bias}(O, \varrho)$, of standard non-mitigated shadow estimation for Pauli observables (see App. B for details) for different system sizes, circuit depths, and in-

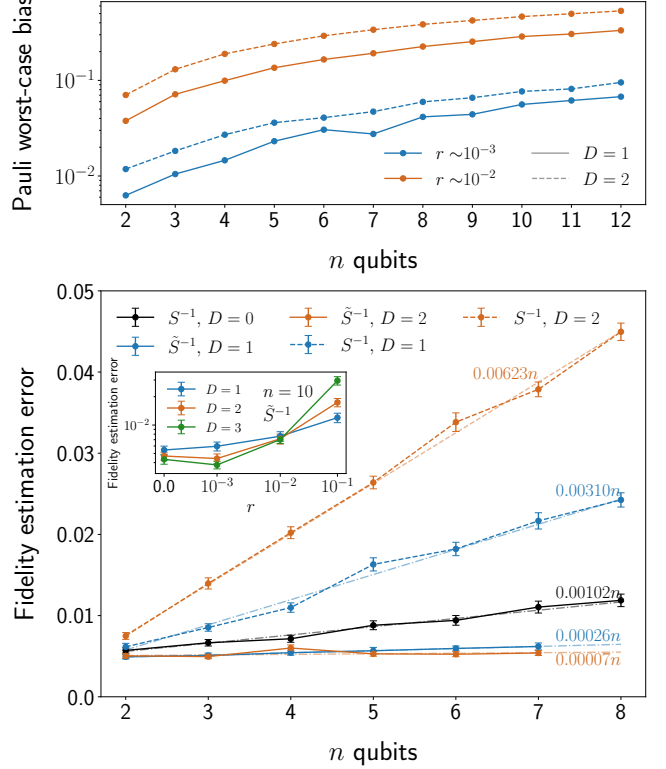


FIG. 2. **Numerical experiments under two-qubit incoherent noise model.** **(top)** Worst-case bias for the estimation of Pauli-observables without mitigation for different system sizes, depth and noise levels. Single-qubit layers sampled from the Haar measure. Noise level indicated by r , the average gate infidelity per CNOT, and samples $|\mathcal{S}| = 10^6$. We observe a sizeable bias about an order of magnitude larger than the two-qubit infidelity and moderately increasing with the system size. **(bottom)** Error in fidelity estimation due to finite statistics $|\mathcal{S}| = 10^5$ for different system sizes, using both \tilde{S}^{-1} and S^{-1} . Single-qubit layers sampled from the Haar measure. The error is averaged over 50 perfectly prepared uniformly-random pure states; errors bars denote the standard error. Noise only affects CNOT gates with $r = 10^{-3}$. We observe a reduction of the system-size dependence and, in consequence, smaller estimation errors for shallow circuit compared to (noiseless) local bases measurements ($D = 0$). The error in unmitigated fidelity estimation grows linearly with n , with a higher slope for increasing depth. In contrast, for mitigates fidelity estimation the slope decreases for increasing depth. **(inset)** Fidelity estimation error using \tilde{S}^{-1} as a function of r for $n = 10$ qubits and $|\mathcal{S}| = 10^5$. We observe a cross-over point at $r = 10^{-2}$; for smaller (larger) infidelities the error decreases (increases) with circuit depth.

coherent noise levels. The worst-case bias is monotonically increasing with all three parameters and the results are consistent with a linear increase of the bias with both the circuit depth and system size. For two-layer shadows, we observe Pauli worst-case biases that are already for three to four qubits about one order of magnitude larger than the average infidelity of the CNOTs used in the cir-

cuit. For example, targeting an estimation precision of 10^{-2} , even fairly accurate CNOTs gates with infidelity 10^{-3} can introduce a sizeable biases in the linear estimation. The stability is improved for Pauli observables with bounded support, see App. D. Nonetheless, without mitigation using even very shallow shadows is often not possible already for small system sizes. This underpins the motivation to study our noise-robust variant.

A key application of shadows with global Clifford rotations is fidelity estimation. Here, the sample complexity is constant in the system size, while randomized local bases measurements have exponential scaling [16]. This leads to the question whether a very shallow hardware-efficient ansatz can improve the sample efficiency even in the presence of experimental imperfections. We simulate the protocol of robust shadow fidelity estimation assuming perfectly prepared pure input states. The fidelity is estimated with respect to the input state itself. Only the two-qubit gate implementing the basis rotation for the shadow suffer from incoherent noise with average infidelity 10^{-3} and the number of samples is fixed to $|\mathcal{S}| = 10^5$. The noisy frame operator is estimated with $|\mathcal{S}| = 10^6$, which we found sufficient for ensuring that the estimation error of \tilde{S} does not limit the accuracy of the fidelity estimation.

Fig. 2 (bottom) shows the estimation error averaged over multiple uniformly-random pure states for different system sizes and circuit depths. We find that the system-size dependence is significantly reduced already for shadows with $D = 1, 2$ when compared to local circuits. In effect, the estimation error is reduced by a factor of about 2 already for these small systems of size $n = 7, 8$ when using short-depth circuits. Importantly, we observe that, in order to harness these effects, the empirical estimation of \tilde{S} put forward here is essential. Without noise-mitigation, the noise-induced bias, depicted in the figure with dashed lines, deteriorates fidelity estimation by factors of 3 to 4 for the same small system sizes and $D = 1$. For $D = 2$ the estimation error using the noiseless frame operator S is already almost one order of magnitude worse than the one that uses \tilde{S} .

In general, even assuming perfect bias mitigation, improving the estimation error by going to deeper circuits will depend on the infidelity of the CNOT gates. Intuitively, every CNOT with incoherent errors will increase the probability that one only learns compromised information about the state. Even if the noise is perfectly mitigated by accurately estimating \tilde{S} , with some probability we learn less about the state. Thus, there will be an increased sample complexity of the fidelity estimation itself. At the same time, longer circuits (without noise) will improve the variance of fidelity estimation eventually reaching the efficacy of 3-designs. We therefore have two competing effects on the sample complexity. We expect that for many estimation tasks there exists a cross-over point depending on the infidelity of the entangling gates.

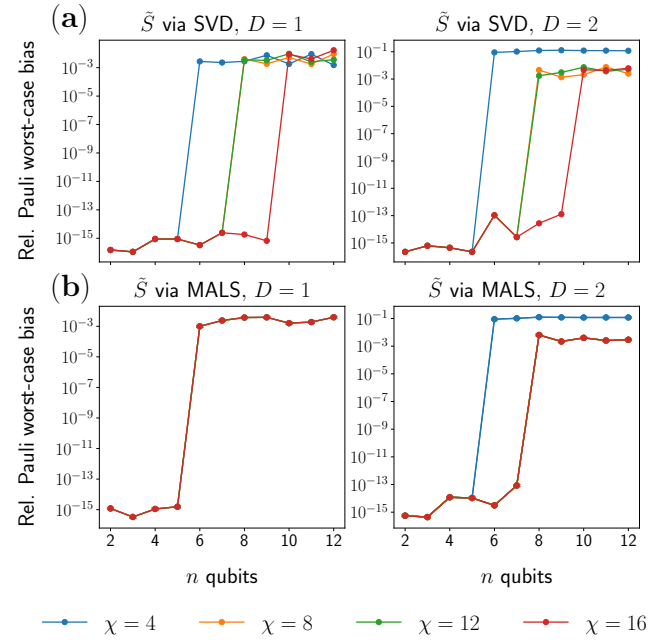


FIG. 3. **Tensor network representation of robust measurement frames of shallow circuits.** (a) Worst-case bias for the estimation of Pauli observables introduced by converting \tilde{S} to a matrix product state (TT) representation using sequential SVDs, relative to the size of the corresponding eigenvalue, as a function of n , for different bond dimensions χ , and depths $D = 1, 2$. We observe that TT ranks 4 and 8 suffice to describe \tilde{S} up-to statistical error. (b) Worst-case bias for the estimation of Pauli observables when learning \tilde{S} directly from the calibration data using a modified ALS method. We find a similar performance as for the sequential SVD.

Below this cross-over infidelity, increasing the depth improves estimation accuracy (at fixed number of samples). Above it, accuracy is deteriorated by deeper circuits.

Using the same fidelity estimation setting as above, we numerically determine the estimation error for different infidelities of the two-qubit gates and circuit depth, averaged over random stabilizer states at fixed system size $n = 10$ and $|\mathcal{S}| = 10^5$. We display such a cross-over in Fig. 2 (inset). We observe that, for infidelities smaller than 10^{-2} , the estimation error using \tilde{S}^{-1} is decreased with circuit depth. For larger infidelities, deeper circuits suffer from large estimation errors. We conclude that indeed even with the robust estimation scheme, deeper shadows being experimentally beneficial is dependent on the noise strength.

We now take a more detailed look at the TT structure of the frame operator and its inverse. We begin with using sequential SVDs to solve the recovery problem in Eq. (6) for different ranks χ using the same noise setting as above. Fig. 3 panel (a) shows the additional (relative) worst-case bias in estimating Pauli observables when using a TT approximation to f instead of the empirically learned dense vector. We indeed find that for $D = 1$

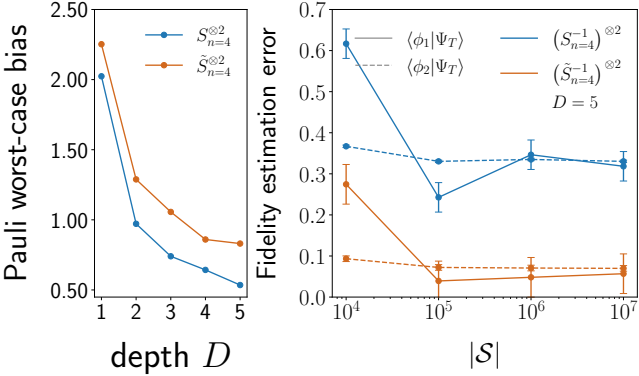


FIG. 4. **Simulation of overlap estimation from Ref. [5] under a gate-dependent noise model.** (left) Worst-case bias for the estimation of Pauli observables introduced by implementing short-depth circuits with and without noise in an experiment, but using the ideal global Clifford frame in the post-processing stage, as a function of D , for two frames: $S_{n=4}^{⊗2}$ (noiseless, blue line) and $\tilde{S}_{n=4}^{⊗2}$ (noisy, brown line). Frames were estimated with $|\mathcal{S}| = 10^6$. Noisy frame was generated under a gate-dependent circuit noise as well as readout noise. (right) Fidelity estimation error using aforementioned frames. States $|\Psi_T\rangle$, $|\phi_1\rangle$, and $|\phi_2\rangle$ are defined in Appendix E.

a rank $\chi = 4$ approximation yields a small relative error that is constant with the system size for $n \geq 6$ and higher ranks do not yield an improvement. Furthermore, we find that for smaller system-sizes the MPS is also fitting the statistical fluctuations. For $D = 2$ we find that $\chi = 8$ accurately approximates \tilde{S} up to statistical error.

We then apply the computationally and storage-efficient MALS algorithm to directly learn a TT representation of \tilde{S} from the shadow data and calculate the induced bias in estimating Pauli observables. We initialize the algorithm with the analytical result for S for the local Clifford frame. We observe an identical performance to the SVD. MALS is rank-adaptive but does not increase the rank beyond $\chi = 8$ for $D = 2$ even if permitted.

Application. As an application, we simulate the quantum experiment of the optimization protocol that was performed on the Sycamore quantum processor in Ref. [5]. The authors prepared an 8-qubit state $|\Psi_T\rangle$ and used classical shadows to estimate the wavefunction overlap $\langle \phi | \Psi_T \rangle$, where $|\phi\rangle$ belongs to a suitable quantum chemistry basis. For the specific choices of $|\Psi_T\rangle$ and $|\phi\rangle$ in our simulations see App. E. The measurement circuit architecture used in Ref. [5] is the 2-fold tensor product of 4-qubit circuits of the same form as Fig. 1. We call the resulting (noisy) frame operator $S_{n=4}^{⊗2}$ ($\tilde{S}_{n=4}^{⊗2}$). Here, the single-qubit rotations are uniformly sampled from the one-local Clifford group. We simulate the experiment using the *gate-dependent* Pauli noise model. More specifically, different single-qubit Clifford gates suffer from different Pauli noise channels. We use the readout error

model for the Sycamore chip described in Ref. [6].

The left panel of Fig. 4 shows, for different circuit depths D , the worst-case bias using shallow shadows as an approximation of shadow estimation using the 2-fold tensor product of the 4-qubit global Clifford group, $S_{\text{gc}, n=4}^{⊗2}$. This is motivated by the strategy of Ref. [5]. We see that $\tilde{S}_{n=4}^{⊗2}$ displays slower convergence to $S_{\text{gc}, n=4}^{⊗2}$ compared to $S_{n=4}^{⊗2}$. This suggests that experimentally performing shallow shadows but analytically inverting $S_{\text{gc}, n=4}^{⊗2}$ for the linear estimation introduces a bias in the estimation. This bias is more pronounced in the presence of (gate-dependent) noise, stressing the necessity to correctly characterize the noisy measurement frame and use its inverse for the estimations. This is presented in the right panel of Fig. 4.

Quantum hardware demonstration. In Fig. 5, we show the results of an experimental implementation of robust shallow shadows on the `ibm_nairobi` quantum processor from IBMQ. We implemented the measurement circuit of Fig. 1 in 5 of the 7 qubits available in the device, for depths $D \in \{0, 1, 2\}$. In Fig. 5 (a) we plot the estimated eigenvalues of \tilde{S} as a function of the cardinality of the shadow $|\mathcal{S}|$ up to $|\mathcal{S}| = 10^5$. (We also provide histograms for the distribution of samples in Fig. 4 (a) in App. F.) For simplicity, we show one eigenvalue per Pauli support. The dashed lines show the eigenvalues of the corresponding noiseless frame. In all three cases, the eigenvalues differ from their noiseless counterparts by a margin that is statistically significant. This confirms that the measurement frame to be inverted in practice should indeed be \tilde{S} instead of S . To cross-validate our results, we separate our 10^5 samples in two batches: with a first batch of 90% of the snapshots, we estimate \tilde{S} ; with the remaining 10%, in turn, we perform a shadow tomography protocol on the 5-qubit state $|0\rangle\langle 0|$ as well as on its marginal state $|0\rangle\langle 0|$ on one of the qubits. For each of the two states, we invert the classical shadows using both \tilde{S}^{-1} and S^{-1} . In Fig. 5 (b), we plot the fidelity biases introduced by the mitigated and unmitigated estimations, respectively. For the unmitigated estimation, one can observe that at $|\mathcal{S}| \approx 10^3$ the statistical error becomes smaller than the bias (i.e., the systematic error due to the ‘wrong’ inverted frame). Increasing the number of samples does not improve the accuracy. In contrast, for the robust shallow shadows, the accuracy continues to increase steadily as $|\mathcal{S}|$ goes beyond 10^3 .

Conclusions. We presented a robust classical shadow scheme for a broad family of noisy, shallow measurement circuits. The measurement calibration stage admits an efficient matrix-product formulation, and the robust inversion stage can also be approximated using standard tensor-network tools. We illustrated the relevance of our method with both numerics and proof-of-principle experiments on an IBM Q device. Numerically, for relevant parameter regimes, we showed that while unmitigated

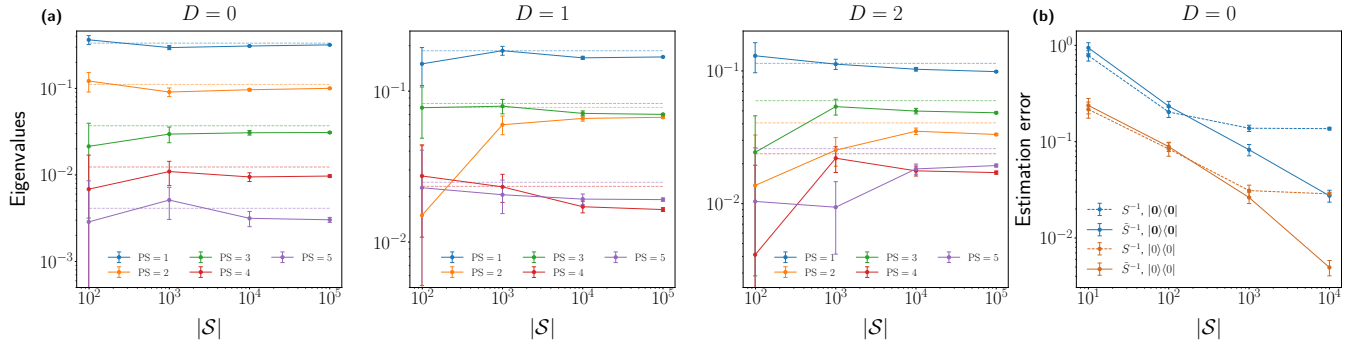


FIG. 5. **Experimental realization on IBM Q.** (a) Eigenvalues of the noisy frame operator \tilde{S} in the Pauli-Liouville basis for $n = 5$ qubits, $D \in \{0, 1, 2\}$, and $|\mathcal{S}| = 10^5$. Error bars correspond to standard errors, i.e. to standard deviations divided by $\sqrt{|\mathcal{S}|}$. We plot one eigenvalue per Pauli support (PS). Dashed lines show the corresponding eigenvalues were the frames noiseless. (b) Cross-validation for $D = 0$ by using shadow tomography to estimate the fidelity of the state preparation of the single-qubit zero state $|0\rangle\langle 0|$ and the n -qubit zero state $|0\rangle\langle 0| \equiv |0\rangle\langle 0|^{\otimes n}$.

shallow shadows with noisy circuits become more biased as the depth increases, robust ones become significantly more accurate up-to a crossing point. Experimentally, in turn, we observed major bias reductions in fidelity estimations using the mitigated variant. Our framework does not require analytical calculations of the effective measurement map but replaces it with a direct estimation protocol. This offers versatile, practical estimation protocols that realize the efficacy of classical shadow as much as it is possible on actually existing and near-term quantum devices by using the available hardware-efficient noisy shallow circuits.

Note added. During the completion of this paper, another independent work [37] appeared that also studies robust shallow shadows.

Acknowledgements. We thank Stefano Carrazza and Stavros Efthymiou for their insights on numerical simulations. We further thank Michał Oszmaniec for discussions on noise mitigation. We thank Jadwiga Wilkens for the availability of the *Quantum Circuit Library* [38].

* renato.msf@gmail.com

- [1] J. Eisert, D. Hangleiter, N. Walk, I. Roth, D. Markham, R. Parekh, U. Chabaud, and E. Kashefi, *Quantum certification and benchmarking*, *Nature Reviews Physics* **2**, 382 (2020).
- [2] M. Kliesch and I. Roth, *Theory of quantum system certification*, *PRX Quantum* **2**, 010201 (2021).
- [3] A. Elben, S. T. Flammia, H. Y. Huang, R. Kueng, J. Preskill, B. Vermersch, and P. Zoller, *The randomized measurement toolbox*, *Nat. Rev. Phys.* **5**, 9 (2022).
- [4] T. Brydges, A. Elben, P. Jurcevic, B. Vermersch, C. Maier, B. P. Lanyon, P. Zoller, R. Blatt, and C. F. Roos, *Probing Rényi entanglement entropy via randomized measurements*, *Science* **364**, 260–263 (2019).
- [5] W. J. Huggins *et al.*, *Unbiasing fermionic quantum Monte Carlo with a quantum computer*, *Nature* **603**, 416 (2022).
- [6] H.-Y. Huang *et al.*, *Quantum advantage in learning from experiments*, *Science* **376**, 1182 (2022).
- [7] S. H. Sack *et al.*, *Avoiding barren plateaus using classical shadows*, *PRX Quantum* **3**, 020365 (2022).
- [8] E. van den Berg, Z. K. Minev, and K. Temme, *Model-free readout-error mitigation for quantum expectation values*, *Phys. Rev. A* **105**, 10.1103/physreva.105.032620 (2022).
- [9] A. Seif *et al.*, *Shadow distillation: Quantum error mitigation with classical shadows for near-term quantum processors*, *PRX Quantum* **4**, 010303 (2023).
- [10] H. Jnane *et al.*, *Quantum error mitigated classical shadows* (2023), arXiv:2305.04956 [quant-ph].
- [11] A. Abbas *et al.*, *On quantum backpropagation, information reuse, and cheating measurement collapse* (2023), arXiv:2305.13362 [quant-ph].
- [12] A. Rath *et al.*, *Entanglement barrier and its symmetry resolution: Theory and experimental observation*, *PRX Quantum* **4**, 010318 (2023).
- [13] B. Vermersch *et al.*, *Enhanced estimation of quantum properties with common randomized measurements* (2023), arXiv:2304.12292 [quant-ph].
- [14] V. Vitale *et al.*, *Estimation of the Quantum Fisher Information on a quantum processor* (2023), arXiv:2307.16882 [quant-ph].
- [15] J. Denzler *et al.*, *Learning fermionic correlations by evolving with random translationally invariant Hamiltonians* (2023), arXiv:2309.12933 [quant-ph].
- [16] H.-Y. Huang, R. Kueng, and J. Preskill, *Predicting many properties of a quantum system from very few measurements*, *Nat. Phys.* **16**, 1050 (2020).
- [17] S. Aaronson and D. Gottesman, *Improved simulation of stabilizer circuits*, *Phys. Rev. A* **70**, 10.1103/physreva.70.052328 (2004).
- [18] H.-Y. Hu, S. Choi, and Y.-Z. You, *Classical shadow tomography with locally scrambled quantum dynamics* (2021), arXiv:2107.04817 [quant-ph].
- [19] K. Bu, D. E. Koh, R. J. Garcia, and A. Jaffe, *Classical shadows with Pauli-invariant unitary ensembles* (2022), arXiv:2202.03272 [quant-ph].
- [20] A. A. Akhtar, H.-Y. Hu, and Y.-Z. You, *Scalable and flexible classical shadow tomography with tensor networks* (2022), arXiv:2209.02093 [quant-ph].

- [21] M. Arienzo, M. Heinrich, I. Roth, and M. Kliesch, *Closed-form analytic expressions for shadow estimation with brickwork circuits* (2022), arXiv:2211.09835 [quant-ph].
- [22] C. Bertoni *et al.*, *Shallow shadows: Expectation estimation using low-depth random Clifford circuits* (2022), arXiv:2209.12924 [quant-ph].
- [23] A. J. Scott, *Tight informationally complete quantum measurements*, Journal of Physics A: Mathematical and General **39**, 13507–13530 (2006).
- [24] D. E. Koh and S. Grewal, *Classical shadows with noise*, Quantum **6**, 776 (2022).
- [25] R. Brieger, I. Roth, and M. Kliesch, *Compressive gate set tomography* (2021), arXiv:2112.05176 [quant-ph].
- [26] E. Onorati, J. Kitzinger, J. Helsen, M. Ioannou, A. H. Werner, I. Roth, and J. Eisert, *Noise-mitigated randomized measurements and self-calibrating shadow estimation* (2024), arXiv:2403.04751.
- [27] S. Chen, W. Yu, P. Zeng, and S. T. Flammia, *Robust shadow estimation*, PRX Quantum **2**, 030348 (2021).
- [28] I. V. Oseledets and S. V. Dolgov, *Solution of Linear Systems and Matrix Inversion in the TT-Format*, SIAM Journal on Scientific Computing **34**, A2718–A2739 (2012).
- [29] W. J. Huggins, S. McArdle, T. E. O’Brien, J. Lee, N. C. Rubin, S. Boixo, K. B. Whaley, R. Babbush, and J. R. McClean, *Virtual Distillation for Quantum Error Mitigation*, Phys. Rev. X **11**, 041036 (2021).
- [30] H.-Y. Hu, R. LaRose, Y.-Z. You, E. Rieffel, and Z. Wang, *Logical shadow tomography: Efficient estimation of error-mitigated observables* (2022), arXiv:2203.07263.
- [31] D. McNulty, F. B. Maciejewski, and M. Oszmaniec, *Estimating quantum hamiltonians via joint measurements of noisy noncommuting observables*, Phys. Rev. Lett. **130**, 100801 (2023).
- [32] H. Jnane, J. Steinberg, Z. Cai, H. C. Nguyen, and B. Koczor, *Quantum Error Mitigated Classical Shadows*, PRX Quantum **5**, 010324 (2024).
- [33] R. J. Garcia, Y. Zhou, and A. Jaffe, *Quantum scrambling with classical shadows*, Physical Review Research **3**, 10.1103/physrevresearch.3.033155 (2021).
- [34] S. F. D. Waldron, *An introduction to finite tight frames* (Birkhäuser New York, NY, 2018).
- [35] A. W. Harrow, *The Church of the Symmetric Subspace* (2013), arXiv:1308.6595 [quant-ph].
- [36] A. Kandala *et al.*, *Hardware-efficient variational quantum eigensolver for small molecules and quantum magnets*, Nature **549**, 242 (2017).
- [37] H.-Y. Hu, A. Gu, S. Majumder, H. Ren, Y. Zhang, D. S. Wang, Y.-Z. You, Z. Minev, S. F. Yelin, and A. Seif, *Demonstration of robust and efficient quantum property learning with shallow shadows* (2024), arXiv:2402.17911 [quant-ph].
- [38] J. Wilkens, *Quantum Circuit Library* (2023).
- [39] Y. V. Fyodorov, *Introduction to the random matrix theory: Gaussian Unitary Ensemble and beyond* (2004), arXiv:math-ph/0412017 [math-ph].
- [40] F. Arute *et al.*, *Quantum supremacy using a programmable superconducting processor*, Nature **574**, 505 (2019).

Appendix A: Incoherent noise model

We model the incoherent noise as an unitary channel $\Lambda := \exp(i\gamma H_g/8)$, where H_g is a random Hamiltonian sampled from the *Gaussian Unitary Ensemble* (GUE) [25, 39], γ is the so-called *strength parameter*, and the constant 8 is a normalization factor (see Sect. IV-B of Ref. [25]). By sampling $H \sim \text{GUE}$, we guarantee that, on average, that is no preferential direction in which the noise acts. Even though $\gamma \in [0, 8]$, we focus on $\gamma < 2$ based on reported error rates for the CNOT gate across multiple commercial quantum computing platforms.

Appendix B: Worst-case bias measure

Consider the case where the half-sided noisy frame operator is still diagonal, i.e. $\tilde{S} = \sum_a \tilde{S}_a |w_a\rangle\langle w_a|$ with $w_a, a \in \mathbb{F}_2^{2n}$, Frobenius-normalized Pauli operators such that $\|w_a\|_F = 1$. We define the bias of standard shadow estimation of an observable from noisy shadow measurements in state ϱ as

$$\text{bias}(O, \varrho) := |(O|\varrho) - (O|S^{-1}\tilde{S}|\varrho)|. \quad (\text{B1})$$

The norm difference $\|S^{-1}\tilde{S} - I\|_\infty$ has the interpretation of the worst-case bias for estimating a single Pauli observable $O_a = \sqrt{d}w_a$. This can be directly seen from the following expression

$$\begin{aligned} \max_{\varrho, a \in \mathbb{F}_2^{2n}} \text{bias}(O_a, \varrho) &= \sqrt{d} \max_{a, \varrho} |(w_a|I - S^{-1}\tilde{S}|w_a)(w_a|\varrho)| \\ &\leq \|I - S^{-1}\tilde{S}\|_\infty, \end{aligned} \quad (\text{B2})$$

where we used diagonality of \tilde{S} in Pauli basis and that $|(w_a|\varrho)| \leq \|w_a\|_\infty \|\varrho\|_1 \leq 1/\sqrt{d}$ for all a, ϱ , and $\|\cdot\|_1$ denoting the trace-norm (nuclear / Schatten-1 norm). Most importantly, this bound is saturated for ϱ in an eigenstate of w_a the observable suffering the maximal bias.

Appendix C: Details on tensor network description

It is well known that each layer of CNOT gates in the hardware-efficient architecture can be written as an MPO with bond dimension $\chi_C = 2$. To see this, we decompose the gate as

$$\begin{aligned} \text{CNOT} &= \sum_{i \in \{0,1\}} |i\rangle\langle i| \otimes X^i \\ &= \left(\sum_{i \in \{0,1\}} |i\rangle\langle i| \otimes \langle i| \otimes \mathbb{1} \right) \left(\mathbb{1} \otimes \sum_{j \in \{0,1\}} |j\rangle \otimes X^j \right) \\ &= (L \otimes \mathbb{1})(\mathbb{1} \otimes R), \end{aligned} \quad (\text{C1})$$

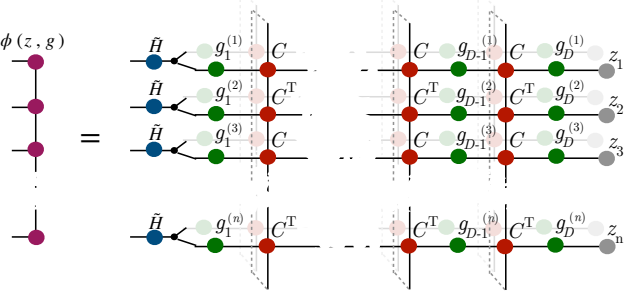


FIG. 6. Tensor network of $\phi(z, g)$. The network in the background is the conjugate of the one in the foreground determined by the measurement outcome z and the applied random single qubit rotations g . The small black dot denotes the copy-tensor, here projecting on the diagonal elements of a density matrix. The matrix \tilde{H} denotes the Hadamard-Walsh transform. Here it is mapping the diagonal elements of the density matrix to the expectation values of multi-qubit Z observables. The entangling layer with MPO core C and C^T has bond dimension 2. As a consequence, the TT rank of $\phi(z, g)$ is 4^D .

where X denotes the Pauli- X gate, and the last line defines the operators L and R . Now we define the MPO core $C_{i,j} := ((i| \otimes \mathbb{1}) R L (\mathbb{1} \otimes |j\rangle) \in \mathbb{C}^{2 \times 2}$. The unitary operator \bar{L}_{CNOT} of a 1D layer of CNOT gates on n qubits with periodic boundary conditions and even n can be written as

$$\sum_{i_1, i_2, \dots, j_1, j_2, \dots} \text{tr} (C_{i_1, j_1} C_{j_2, i_2}, C_{i_3, j_4} \dots C_{i_{n-1}, j_n}) |j_1, j_2, \dots \rangle \langle j_1, j_2, \dots|. \quad (\text{C2})$$

By construction, L_{CNOT} is an MPO of bond dimension 2. As a consequence $\phi(z, g) = (\phi_k(z, g))_{k \in [n]}$, illustrated in Fig. 6 is a TT of bond dimension at most $\chi_C^{2D} = 4^D$.

The operator \tilde{S} can also be written as a shallow circuit of operators acting on quantum channels. Assuming local invariance, also $f = (f_k)_{k \in [n]} \in \mathbb{R}^n$ has a corresponding circuit representation. The rank of the resulting TT description of f is increased by every layer of entangling gates and non-local noise. For fairly general noise affecting the shallow circuits, f is of low TT rank. To this end, it is instructive to discuss a scenario with strictly local and mostly gate-dependent noise. Let us assume that $\Omega_j^{(i)}(U)$ is the CPT map describing the noisy implementation of the gate $U \in \text{U}(2)$ when applied on qubit i in the circuit layer j . This noise model is general enough to also capture local noise and errors affecting the read-out and entangling gates. These noise effects can be included in the respective neighbouring layer of single-qubit rotations. The local channel twirl with a group G including noise is formally described by the non-commutative Fourier transform of the map $\Omega_j^{(i)}$ evaluated at the representation of unitary channels $\omega(U) = U \otimes \bar{U}$, i.e.

$$\hat{\Omega}_j^{(i)}[\omega] = \int_G \bar{U} \otimes U \otimes \Omega_j^{(i)}(U) d\mu(U). \quad (\text{C3})$$

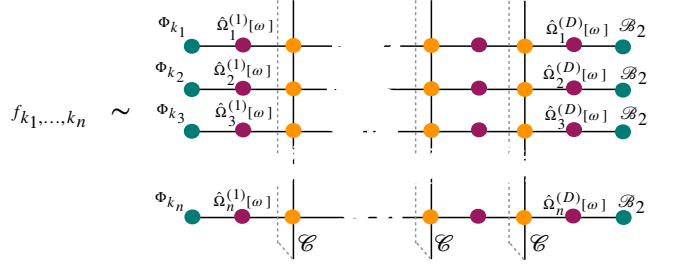


FIG. 7. Tensor network of f for strictly local noise mostly gate-dependent noise. The entangling layer acting here as a ‘super-duper operator’ on quantum channels has MPO bond-dimension 16, restricted to Pauli noise channels it has MPO bond dimension 4. Correspondingly, the TT rank of f is 16^D for local noise and 4^D for local Pauli noise.

We will here simply use $\hat{\Omega}_j^{(i)}[\omega]$ as convenient symbol for the “noisy channel twirl”. Note that $\hat{\Omega}_j^{(i)}[\omega]$ is a linear operator on superoperators, a “super-duper-operator” if one insists. We can also introduce a corresponding operator for the entangling layer that conjugates a quantum channel with unitary channels of layer of CNOT gates. The resulting MPO, $\mathcal{C} = \bar{L}_{\text{CNOT}} \otimes L_{\text{CNOT}} \otimes L_{\text{CNOT}} \otimes \bar{L}_{\text{CNOT}}$, has bond dimension 16. The read-out is locally described by $\mathcal{B}_2 = \sum_{z \in [2]} |\Pi_z\rangle \langle \Pi_z|$, the local dephasing channel in computational basis. Finally, to ensure the local invariance of \tilde{S} , we assume gate-independent left noise $\Omega_j^{(1)}(U) = \Lambda_j \omega(U)$ for the first layer acting on the state under consideration, with Λ_j being a quantum channel.

Figure 7 depicts the resulting expression for f . Without any further assumption, we conclude that f has TT rank of at most 16^D . The rank is even smaller if all noise channels are Pauli noise. Then, we can fully restrict the circuit in Fig. 7 as acting only on the subspace of Pauli noise channels, i.e. diagonal channels in Pauli operator basis. To see this note that the local dephasing channel is a Pauli noise channel. Under the assumption of Pauli noise, the noisy channel twirl maps Pauli noise channels to Pauli noise channels. Being a Clifford unitary, the entangling layer acts as a two-local permutation on the diagonal of the Pauli-noise channel. The representation of \mathcal{C} restricted to Pauli-noise channels has (MPO) bond dimension 4. Hence, f is described by an TT of rank at most $\chi = 4^D$.

The argument for one-local noise can be generalized to quasi-local noise by introducing, e.g., MPO descriptions of the implementation map modelling cross-talk effects, or modelling a noisy entangling layer \mathcal{C} with a potentially larger bond dimension. In general, the TT rank of f will be increased due to correlated noise effects. If these correlations are sufficiently short-ranged, f still has an effective low-rank description. We expect that this will often be the case on actual quantum hardware.

Appendix D: Worst-case bias per Pauli support

In Figure 8 we show the same worst-case bias of standard non-mitigated shadow estimation for Pauli observables, under the same noise conditions. This is presented in shaded lines. However, this time we also present the worst-case bias for fixed Pauli supports $PS = 1, 2$. We observe that the Pauli worst-case biases for these Pauli supports seem to hit a plateau for both noise levels. However, for $r \sim 10^{-2}$, even though stable, the biases are still sizeable.

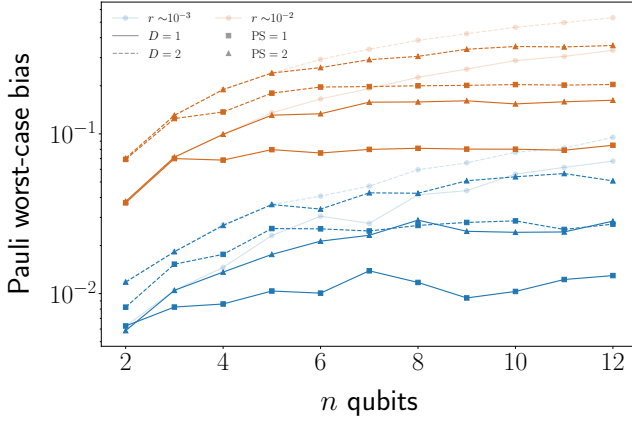


FIG. 8. Worst-case bias from Fig. 2 for different Pauli supports.

Appendix E: Overlap estimation based on Ref. [5]

The optimization protocol for quantum chemistry problems implemented by Ref. [5] involves estimating the wavefunction overlaps $\langle \phi | \Psi_T \rangle$. This is done by preparing $|\Psi_T\rangle$ in a quantum processor, constructing its classical shadow representation, and evaluating the overlap with multiple $|\phi\rangle$ via post-processing. The state $|\Psi_T\rangle$ is called a *trial function*, and $|\phi\rangle$ is named a *walker function*. We refer to Ref. [5] for more details about $|\Psi_T\rangle$ and $|\phi\rangle$ in

the quantum chemistry context. For our intents and purposes, we set a phase $\theta = \pi/\sqrt{2}$, and

$$|\Psi_T\rangle = \cos^2(\theta) |11001100\rangle + \frac{1}{2} \sin(2\theta) |11000011\rangle + \frac{1}{2} \sin(2\theta) |00111100\rangle + \sin^2(\theta) |00110011\rangle. \quad (E1)$$

Moreover, we define

$$|\phi_1\rangle = \frac{1}{2} |11001100\rangle + \frac{1}{2} |11000011\rangle + \frac{1}{2} |00111100\rangle + \frac{1}{2} |00110011\rangle. \quad (E2)$$

and

$$|\phi_2\rangle = \frac{1}{\sqrt{2}} |11001100\rangle + \frac{1}{\sqrt{6}} |11000011\rangle + \frac{1}{\sqrt{6}} |00111100\rangle + \frac{1}{\sqrt{6}} |00110011\rangle. \quad (E3)$$

We simulate the perfect preparation of $|\Psi_T\rangle$ and its reconstruction via classical shadows with noisy measurements. The noise model chosen is based on the one from the Sycamore processor [6, 40], since Ref. [5] implements this protocol in that quantum hardware.

Appendix F: Data histograms for Fig. 5 (a)

As explained in the main text, given the sequence \mathcal{S} of snapshots obtained using the quantum hardware, the k -th eigenvalue of the noisy frame operator \tilde{S} is estimated by calculating $\mathbb{E}_{(z,g) \in \mathcal{S}} \phi_k(z, g)$, $\forall k$, with ϕ_k being defined in Eq. (5).

Here, we present the distributions of the data used to estimate the eigenvalues of the noisy frame operator obtained on the `ibm_nairobi` quantum processor using the IBMQ platform. As in Fig. 5 (a), we show one eigenvalue per Pauli support PS and per depth $D \in \{0, 1, 2\}$. Moreover, we use a sequence of size $|\mathcal{S}| = 10^5$.

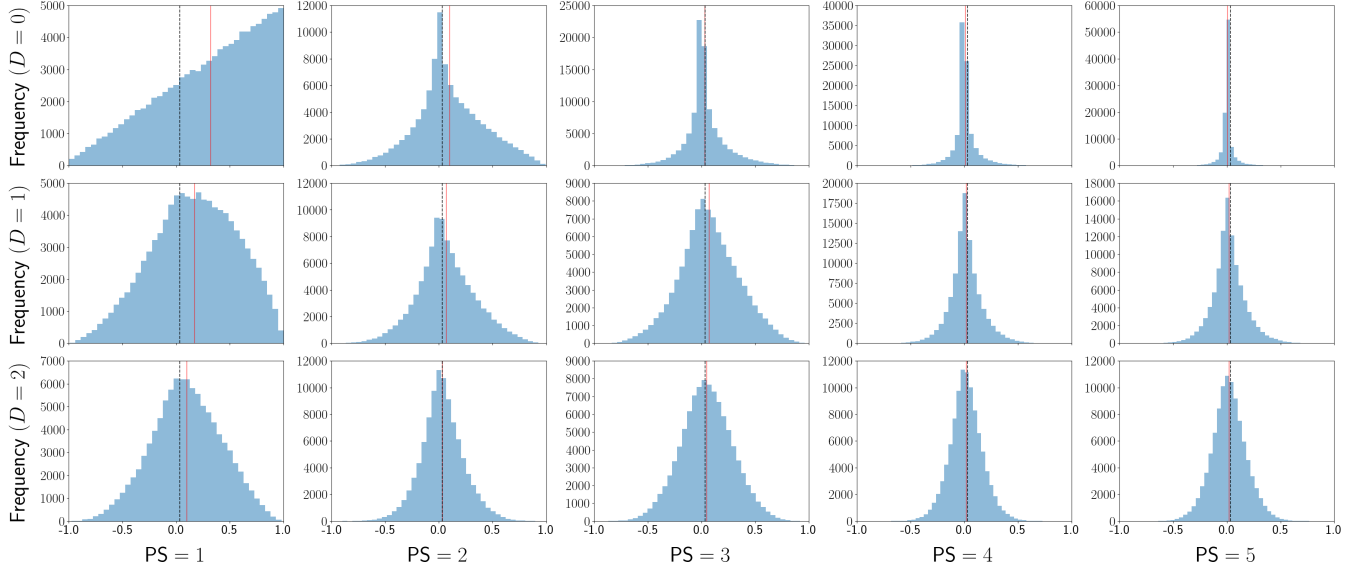


FIG. 9. **Histograms of experimental realization on IBMQ.** Distribution of samples used to estimate eigenvalues of the noisy frame \mathcal{S} for different Pauli supports $1 \leq \text{PS} \leq 5$, over $|\mathcal{S}| = 10^5$ samples from the `ibm_nairobi` quantum processor, for $n = 5$ and $D \in \{0, 1, 2\}$. The average over the 10^5 samples gives our estimates of the eigenvalues of $\tilde{\mathcal{S}}$ shown in Fig. 5 (a). We indicate the corresponding eigenvalue by dashed red lines, while the dashed black lines indicate the $1/(d+1)$ level.